

Engineering charge transport by heterostructuring solution-processed semiconductors

Oleksandr Voznyy*, Brandon R. Sutherland*, Alexander H. Ip*, David Zhitomirsky and Edward H. Sargent

Abstract | Solution-processed semiconductor devices are increasingly exploiting heterostructuring — an approach in which two or more materials with different energy landscapes are integrated into a composite system. Heterostructured materials offer an additional degree of freedom to control charge transport and recombination for more efficient optoelectronic devices. By exploiting energetic asymmetry, rationally engineered heterostructured materials can overcome weaknesses, augment strengths and introduce emergent physical phenomena that are otherwise inaccessible to single-material systems. These systems see benefit and application in two distinct branches of charge-carrier manipulation. First, they influence the balance between excitons and free charges to enhance electron extraction in solar cells and photodetectors. Second, they promote radiative recombination by spatially confining electrons and holes, which increases the quantum efficiency of light-emitting diodes. In this Review, we discuss advances in the design and composition of heterostructured materials, consider their implementation in semiconductor devices and examine unexplored paths for future advancement in the field.

Solution-processed semiconductors have the potential to realize low-cost, large-area, mass-manufacturable optoelectronic devices on flexible substrates. Semiconductor precursors that are dispersed in a solvent can be cast into solid-state films through various techniques, including spin coating, inkjet printing and spray coating. This is in stark contrast to conventional epitaxial inorganic semiconductor materials fabrication, which requires complex high-temperature processing methods, such as Czochralski growth or metal–organic chemical vapour deposition. The three primary classes of solution-processed materials are semiconducting organics, colloidal quantum dots (CQDs) and metal halide perovskites. Today, state-of-the-art devices made from these materials can achieve performances that approach or exceed those of epitaxially grown inorganic single-crystal semiconductor devices.

These three classes of semiconductors span a range of materials with a diverse set of physical, optical and electronic properties that are primarily determined by their intrinsic carrier mobility (μ) and exciton binding energy (E_b), as illustrated in FIG. 1. The interplay between mobility and exciton binding energy in solution-processed materials dictates the guidelines for the design of efficient light-emitting and light-harvesting devices.

In this Review, we show how heterostructuring in optoelectronic devices based on organics, CQDs and perovskites overcomes materials limitations to achieve high efficiency. In addition, we discuss the roles of mobility and exciton binding energy in disordered semiconductors and how they govern the motion of charge carriers, we analyse recent advances in heterostructured materials for light-harvesting and light-emitting semiconductor devices, and we provide a critical evaluation of paths for future developments.

Semiconducting organic materials include both polymer and small-molecule systems¹. Early demonstrations of high-conductivity halide-doped polyacetylene inspired a new field of solution-processed semiconductor devices². Progress in materials synthesis enabled the realization of solution-processed organic light-emitting diodes (OLEDs)³, lasers⁴ and solar cells⁵. Building on this pioneering work, solution-processed organic semiconductors have now demonstrated LED external quantum efficiencies (EQEs) in excess of 20%⁶ and solar cell power conversion efficiencies (PCEs) of more than 12%⁷.

CQDs are solution-processed materials systems that consist of semiconductor nanocrystals that are a few nanometres in diameter. The theoretical framework for

Department of Electrical and Computer Engineering, University of Toronto, 10 King's College Road, Toronto, Ontario M5S 3G4, Canada.

*These authors contributed equally to this work. Correspondence to E.H.S. ted.sargent@utoronto.ca

doi:10.1038/natrevmats.2017.26
Published online 23 May 2017

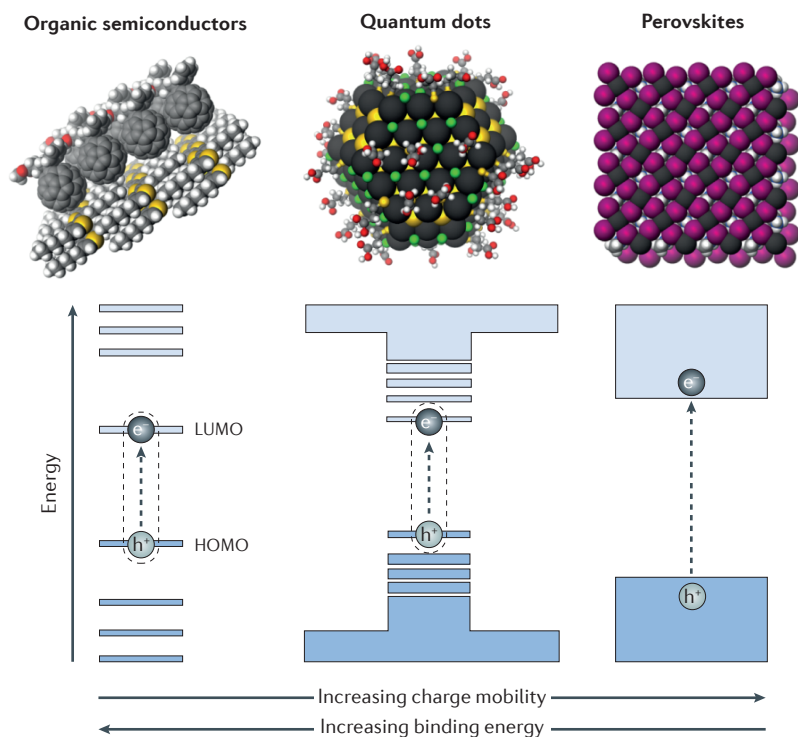


Figure 1 | Electronic properties of organic semiconductors, quantum dots and perovskites. Electronic properties are determined by the degree of quantum confinement, which affects the density of states, exciton binding energy and charge mobility. HOMO, highest occupied molecular orbital; LUMO, lowest unoccupied molecular orbital.

these crystallites was developed in the 1980s^{8,9}, revealing a dependence of bandgap on nanocrystal size. Early synthesis of monodisperse cadmium-based chalcogenide CQDs¹⁰ inspired the development of new precursors and synthetic routes to further enable high-quality nanocrystals based on lead¹¹ and indium¹². The addition of epitaxial shells during synthesis enabled high luminescence efficiency from CQDs for the first time¹³, suggesting promise for efficient light-emitters, which are now being realized. CQDs were proposed as promising materials for third-generation solar cells, owing to their potential for hot-carrier extraction and multi-exciton generation¹⁴. Today, the cadmium-family of CQDs is extensively used in light-emitting systems, including LEDs with EQEs of more than 20%¹⁵ and quantum-well lasers that operate under continuous-wave pump excitation¹⁶. State-of-the-art lead-based CQDs are applied as the active layer in photovoltaic cells with PCEs in excess of 11%¹⁷ and infrared photodetectors¹⁸.

Metal halide perovskites are a class of direct-bandgap bulk semiconductor that can be solution processed owing to the solubility of the halide-based precursors. Although the term ‘perovskite’ refers to a general crystal structure, we use the term herein for brevity to describe the family of solution-processed semiconducting metal halide perovskites. Early studies in the 1990s demonstrated that perovskite materials can exhibit high field-effect-transistor mobilities¹⁹ and bright electroluminescence²⁰. More than two decades later, interest in this material was revived after its discovery as an efficient solar-harvesting

material that rapidly achieved PCEs above 10%²¹. Today, perovskites exhibit PCEs of greater than 20%^{22,23} and have further expanded their applicability as efficient emitters in LEDs with EQEs approaching 12%^{24–26}.

Charge extraction and injection

The architectural design considerations for optoelectronic devices that have application in light harvesting or light emission are fundamentally different. Correspondingly, the semiconductor materials that comprise the active layers in these devices have opposite functions. In this section, we outline guidelines for the design of active materials in systems that are tailored for either the absorption or generation of light. We base this framework around the interplay between carrier mobility and exciton binding energy in disordered semiconductors and discuss how the presence of defect states affects these design rules.

Mobility is a measure of the speed of a charge carrier as it moves through a conductive medium in the presence of an electric field. Exciton binding energy is a measure of the strength of interaction between an electron and a hole. Both parameters are important electrical properties of semiconductors and directly influence the efficiency of optoelectronic devices by influencing carrier recombination (FIG. 2). There are three main types of recombination in semiconductor materials and devices: non-radiative recombination at defects, radiative recombination and non-radiative Auger recombination. For high-efficiency devices, the properties of the active material should be tuned to favour either radiative recombination or carrier extraction; in all cases, undesirable non-radiative recombination losses must be suppressed.

Defects are inevitably present in any material and are of crucial importance in disordered solution-processed materials in which their abundance often directly limits device performance. Most defects induce localized energetic states within the bandgap, called electronic traps. Free carriers can become captured in traps, and once a carrier of the opposite charge arrives at the same trap, they recombine non-radiatively (FIG. 2a). The probability of such recombination depends on the density of the defects and their capture cross-section; the total amount of losses scales linearly with carrier concentration²⁷. In the absence of traps, carriers would eventually meet and recombine radiatively (FIG. 2b).

Radiative recombination is the process by which an electron relaxes from the conduction band to the valence band with the emission of light at the transition energy. The radiative recombination rate is proportional to the overlap of the electron and hole wavefunctions. Therefore, efficient radiative recombination requires electrons and holes to meet and remain in a localized volume for a period longer than the radiative lifetime. Strongly interacting electrons and holes form excitons with large binding energies and remain co-localized, resulting in a higher probability of light emission (FIG. 2c). At the other extreme, when electrons and holes are non-interacting and become free, an increase in the carrier concentration will increase the probability that carriers will meet and recombine; this gives rise

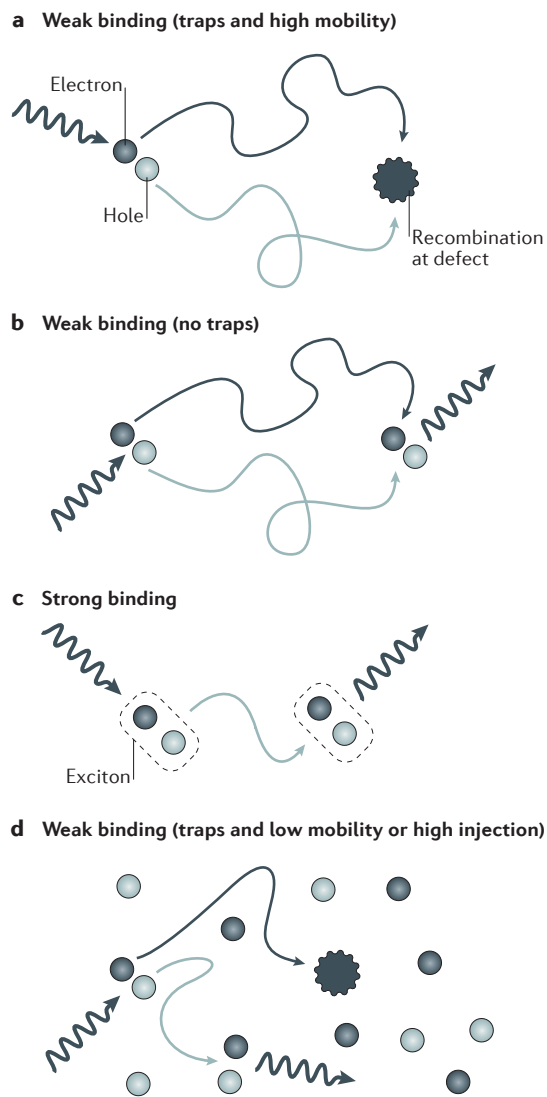


Figure 2 | Recombination mechanisms. Illustrations showing the mechanisms for the recombination of electrons and holes; the mechanism depends on the interplay between the exciton binding energy and the charge carrier mobility. **a** | When traps are present, free carriers find traps faster than they can meet again. **b** | When binding is weak, excitons can dissociate into free carriers, but can eventually meet again and recombine. **c** | In the case of strong binding, excitons can diffuse a short distance before recombining radiatively. **d** | When mobility is low, carriers accumulate in the material because they are not extracted sufficiently quickly, reaching a population higher than that of traps, thus making radiative recombination more probable.

to a quadratic dependence of radiative recombination efficiency on carrier concentration (FIG. 2d).

Auger recombination is a higher-order process that occurs when an electron and hole recombine and transfer the excess energy to a nearby carrier. In organic semiconductors, it is known as triplet–triplet annihilation and leads to the creation of a new singlet state. This process annihilates the electron–hole pair without generating a photon and is thus a non-radiative loss. Similar to

radiative recombination, Auger recombination requires a strong overlap of the electron and hole wavefunctions. The presence of a third carrier is a necessary requirement, which makes Auger recombination noticeable only under high carrier densities; however, it quickly becomes the dominant recombination pathway owing to its cubic dependence on carrier concentration.

In applications that require efficient charge extraction (for example, solar cells and photodetectors), each of the types of recombination mentioned above should be suppressed; by contrast, in light-emission applications, radiative recombination should be maximized whereas defect- and Auger-mediated recombination should be avoided. A particular recombination pathway can be enhanced by tuning the basic materials properties such as trap density, carrier mobility and exciton binding energy.

All solution-processed materials share some common features. Low-temperature processing generally means that there is a high chance of defect formation. The high surface area and porosity of disordered materials facilitate the penetration of oxidizing molecules (such as oxygen and water) into the structure. This creates additional electronic traps and often alters the doping levels of the material. Depending on the material, doping can either fill in the traps and provide a smoother energy landscape for electronic carriers or, by contrast, facilitate the formation of defects that counteract the effect of doping in a process called self-compensation. Reducing the density of traps is thus a crucial requirement in the synthesis of high-performance semiconductor materials.

Another common result of solution processing is a high degree of structural disorder. This leads to an inhomogeneous energy landscape that indirectly affects the mobility of carriers. In organic semiconductors, it mainly arises from the disorder in the orientation and structural conformation of the molecules. In CQD films, it stems from size polydispersity, which affects the degree of quantum confinement in each nanocrystal. In perovskites, it is a result of non-uniform crystalline domains that are separated by grain boundaries. These inconsistent energy landscapes can lead to preferential concentration of carriers in low-energy ‘hotspots’, which promotes radiative and Auger recombination.

Despite their similarities as solution-processed materials, organic, CQD and perovskite materials vary considerably in terms of carrier mobility and exciton binding energy (TABLE 1). Strong exciton localization and low permittivity enhances the electron–hole interactions in organic molecules, as reflected in the respective exciton binding energies ($E_b > 100$ meV); intermediate quantum confinement effects occur in CQDs and 2D perovskites ($E_b \approx 20$ – 200 meV); and electron–hole interactions are virtually non-existent in bulk perovskites with strong dielectric screening ($E_b \approx 25$ meV). Carrier mobility is usually much lower in organics, intermediate in CQDs and high in perovskites. Improved crystallinity within the organic films²⁸, reduced CQD size distribution¹⁷ and improved coupling between individual CQDs (often through partial fusion)^{29,30} can increase the mobility in both organics and CQDs to values that are comparable with those of perovskites (>10 cm² V⁻¹ s⁻¹).

Table 1 | Optoelectronic parameter ranges for solution-processed organic, CQD and perovskite materials

Material	Limiting mobility, μ ($\text{cm}^2 \text{V}^{-1} \text{s}^{-1}$)	Exciton binding energy, E_b (eV)	Transport control
Organics	10^{-4} – 10^{-3} (REF. 103)	0.1–1 (REF. 104)	Choice of polymer or molecule, tuning of the functional end groups
CQDs	10^{-3} – 10^{-2} (REF. 105)	0.1–0.3 (REFS 47,106)	Size-tuning, dot coupling via ligands
Perovskites	1 – 10^2 (REF. 107)	0.01–0.2 (REF. 108)	Compositional tuning, quantum confinement

CQD, colloidal quantum dot.

The interplay between exciton binding energy and mobility determines the rate of exciton dissociation and thus the rate of radiative recombination. In the absence of competing recombination losses, carriers can meet and recombine radiatively even after exciton dissociation (FIG. 2b). However, the presence of traps, even in small amounts, provides a competing recombination channel (FIG. 2a). Therefore, to enhance the radiative rate, strong exciton binding and/or low mobility (FIG. 2c,d) are preferred in light-emitting materials. However, decreasing mobility can be effective only to a certain extent: at some point, it leads to the accumulation of carriers that activates Auger recombination, which out-competes the radiative channel. This is particularly true in devices with thicker light-emitting active layers, which are desirable for higher brightness. Low mobility complicates carrier injection and leads to an imbalanced accumulation of electrons on one side of the device and holes on the other, which favours Auger over radiative recombination.

When efficient charge extraction is required, weak binding and high mobility (FIG. 2a) are necessary to suppress radiative recombination, which now represents a loss. Higher mobility can in some cases also reduce the recombination through traps by reducing the time for a carrier and a trap to interact or by enhancing the escape rate from shallow traps, but in most cases it only speeds up the trapping; thus, an optimal value of mobility is usually sought.

The above requirements would seem to restrict each material class — when used in its pure phase — to a particular application. Purely organic materials do not seem to be suited for carrier extraction because of the high radiative losses, whereas perovskites, owing to the high carrier mobility, have poor chances of emitting light. Even when the mobility and exciton binding energy can be tuned, a compromise has to be made between Auger and trap losses, which can never be completely eliminated. In the following section, we describe how this compromise can be overcome by implementing heterostructuring within each material system and how a combination of two disparate materials can benefit from the positive qualities of the individual materials.

Heterostructuring Efficient charge extraction

To develop high-efficiency solution-processed photovoltaics, it is important to increase the carrier diffusion length, which is limited by high defect densities or high radiative losses. In organic semiconductors, losses are dominated by radiative recombination owing to the

strong interaction between electrons and holes, which leads to stable excitons. In quantum dots and perovskites, excitons easily dissociate into free carriers that recombine when they meet at defect sites. Therefore, decreasing the density of traps is a pervasive research topic in solution-processed materials. Progress on this front requires significant improvement in materials quality. However, an alternative approach for minimizing losses is to separate electrons and holes into different phases with the aid of heterostructuring, specifically, intermixing two materials with a staggered band alignment, as shown in FIG. 3.

Bulk heterojunctions (BHJs) in organic materials facilitate rapid charge separation of photogenerated excitons at interfaces³¹, thereby preventing geminate radiative (Langevin) recombination (FIG. 3a) and subsequently enabling the transport of electrons and holes through separate phases. For this approach to be successful, the energy offset between the two materials must be sufficient to overcome the exciton binding energy. The distance between the constituent phases should be shorter than the diffusion length of the exciton (typically of the order of 10 nm) (FIG. 3b) to ensure the separation of excitons before they recombine.

It is also important that each phase is continuous to ensure that carriers can reach the electrodes unimpeded (FIG. 3c). The interactions between organic materials and additives in the solutions used for processing have been widely explored and have been shown to influence phase separation^{32–34}, domain size and domain shape. It is preferred that each phase retains its crystallinity, which requires precise control over film formation by appropriate choice of solvents and processing temperatures. The crystallinity also determines the offset energy of the bands. Ultrafast spectroscopy shows that crystalline phases allow for electron delocalization over a larger volume, which reduces the exciton binding energy³⁵.

The BHJ strategy has been the key to the success of organic solar cells^{36–39}, which have now reached certified efficiencies in excess of 12%⁷. The BHJ strategy has been extended to other systems that suffer from short diffusion lengths, including inorganic nanocrystals^{40–42} and hybrid polymer–nanocrystal devices^{43,44}. In the latter case, controlling the extent of the CQD domains is a major challenge^{40,42,45,46}, and the use of nanorods that span the thickness of the whole device is one effective approach to address this problem⁴⁴ (FIG. 3d).

Shell-free quantum dot films were shown to be non-excitonic, rapidly dissociating into free carriers, when the initial oleic acid ligands were exchanged to

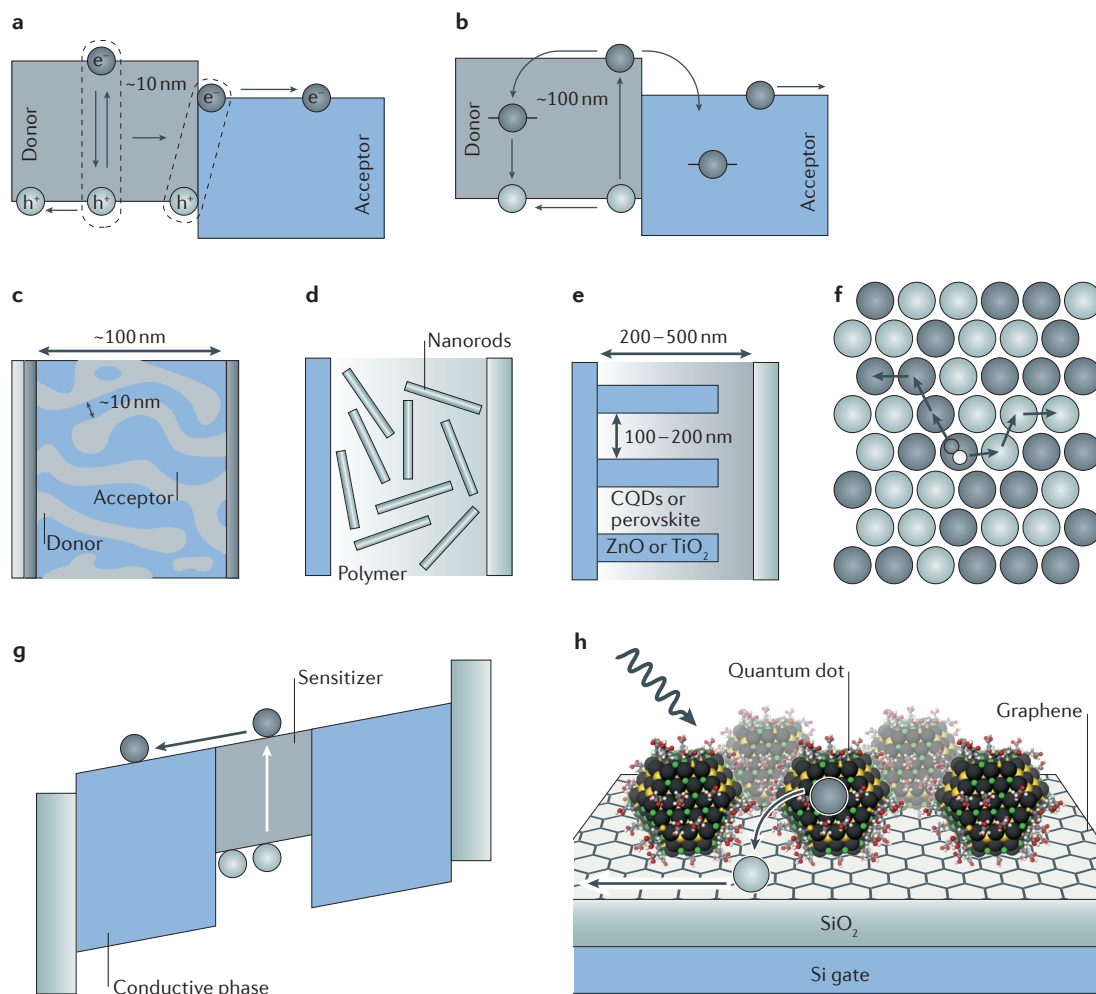


Figure 3 | Charge extraction in heterostructured materials. **a** | Energy band diagram of a bulk heterojunction for excitonic materials, indicating bimolecular recombination as the main loss. **b** | Energy band diagram of a bulk heterojunction for the case of free carriers, showing trap recombination as the main loss. **c** | Structure of a typical bulk heterojunction used in organic photovoltaics^{36–39}. **d** | Bulk heterojunction mixing of a polymer and inorganic nanorods⁴⁴. **e** | Bulk heterojunction using nanoneedles that penetrate into the colloidal quantum dot (CQD) or photoabsorbing perovskite phase^{61,62}. **f** | A homogeneous mixture of donor- and acceptor-type quantum dots acting as a bulk heterojunction. **g** | Band diagram of a material with asymmetric electron and hole extraction used in photodetectors. **h** | Example of a photodetector based on PbS quantum dots as a sensitizer and graphene as a high-conductivity phase⁷⁰.

shorter thiols⁴⁷. This is a result of the high carrier mobility and small exciton binding energy within these systems, which eliminates radiative losses. However, higher mobility does not improve charge extraction in the presence of trap states; it only speeds up the capture of carriers into traps, leaving the diffusion length of the carriers unaffected⁴⁸. Indeed, the ligand-exchange procedure often leads to quantum-dot aggregation and necking, which increases the energetic disorder^{17,49,50} and even the density of traps⁴⁸.

To improve the surface passivation in quantum-dot films, retention of the original ligands or growth of passivating shells^{51,52} is desired, if this can be achieved without significantly reducing the carrier mobility. A judicious choice of ligand can reduce the barrier for carrier transport and retain the conductivity of an organic–quantum dot composite if the highest

occupied or lowest unoccupied molecular orbital level of the ligand is aligned with that of the quantum dot solid^{53–55}, even for relatively long ligands. Another alternative, which has been the most successful approach to date, is to perform a ligand exchange in the solution phase, imposing less damage to the surface^{17,56–59}. Nevertheless, defects and the effects they have on carrier diffusion length remain the key limiting factors in quantum dot optoelectronics, and a BHJ architecture still holds promise for improving these materials (FIG. 3b). Free carriers are still able to get trapped at defects when separated into different phases; however, to recombine, the carrier of the opposite charge must arrive at the same trap. If this does not happen, the trap becomes filled and cannot accept more carriers of the same charge in accordance with the Pauli exclusion principle.

Various combinations of nanomaterials have been tested in BHJ architectures: from macroscopic well-defined continuous TiO₂ nanopillars⁶⁰ and ZnO nanowires^{61,62} (FIG. 3e) to homogeneously mixed quantum dots of different composition and size^{41,42,45}. The benefit of quantum dots over organics is that they do not require a continuous phase of the same material. Instead, with a sufficient concentration of nearest neighbours of the same identity, high carrier mobility can be sustained even when multiple types of quantum dot are homogeneously mixed (FIG. 3f). In organic materials, such random mixtures become too disordered, preventing efficient carrier transport. The compatibility of solvents and the passivation of the two materials that constitute the BHJ remain challenging, preventing these heterostructured architectures from outperforming planar quantum-dot devices.

The first promising photovoltaic performance achieved with halide perovskites relied on a BHJ with mesoporous TiO₂ (REFS 63,64). Heterostructured perovskite-PCBM (phenyl-C₆₁-butyric acid methyl ester) films showed potential in hysteresis-free high-efficiency solar cells. In this case, PCBM serves at least two functions: it acts as an efficient electron acceptor, forming a continuous conductive phase for electrons, and it passivates grain boundaries in a similar way to that of other organic additives⁶⁵. After intensive efforts, researchers have shown that carrier diffusion lengths in perovskites are both balanced and long; through proper synthetic control^{66–68} diffusion lengths can now reach several micrometres. Today, the performance of planar perovskite solar cells⁶⁹ approaches that of the best heterostructured counterparts²².

In addition to providing a means to overcome the short carrier diffusion length in solar cells, heterostructured materials also have an advantage in photodetectors. In photoconductive light sensors, the temporary trapping of a carrier in a localized phase can delay its extraction (FIG. 3g). When coupled with a highly conductive phase for the carrier of the opposite polarity, such carrier imbalance enables photoconductive gain. PbS quantum dots have been demonstrated as effective photosensitizers in combination with graphene⁷⁰ (FIG. 3h) and C₆₀ single crystals⁷¹ as conductive phases. In a recent example, PbS quantum dots were used to efficiently delay carriers in highly conductive perovskites⁷²; in this work, non-radiative recombination was avoided as a result of effective lattice matching and passivation between the perovskite phase and the quantum dots⁷³. In another study, slowing down the carriers inside the perovskite required organic additives that introduced disorder and reduced the quality of the perovskite⁷⁴. The asymmetric conductivity of carriers has also been demonstrated using CdSe quantum dots with CdS shells. Owing to a quasi-type II band alignment, holes are efficiently trapped inside the quantum dot cores whereas electrons are free to move between the dots (FIG. 3g). Ligand exchange with metal chalcogenide complexes shortened the inter-dot distance, further enhancing electron mobility⁷⁵.

Enhanced radiative recombination

Light-emitting devices, such as LEDs, require an active medium with a high radiative recombination rate, which, as mentioned above, is proportional to the overlap of the electron and hole wavefunctions. For materials with a high carrier mobility — and consequently a low exciton binding energy — such as perovskites, the delocalization of carriers limits this rate. By contrast, materials with a high exciton binding energy, such as organic materials and CQDs, have inefficient and imbalanced carrier transport across thick active layers; this limits the radiative rate by impeding the spatial overlap of injected carriers. LEDs require both high and balanced carrier mobilities and high exciton binding energies — something that is not realized in homogeneous materials with flat energy landscapes. Therefore, to achieve high-efficiency LEDs researchers have exploited heterostructuring. In this section, we examine the heterostructured materials design of LEDs based on emitting layers of organic semiconductors, CQDs or perovskites. These are termed OLEDs, QD-LEDs, and PeLEDs, respectively. We emphasize the less-studied and emerging QD-LED and PeLED materials systems.

Solution-processed LEDs break the mobility versus binding energy compromise by utilizing type I heterojunctions to spatially confine injected charge carriers (FIG. 4a). In an ideal implementation of this system, the constituent with the wider bandgap has large ambipolar mobilities (that is, balanced electron and hole mobilities) and is a continuous phase for effective transport. The energetic confinement of the component with the smaller bandgap provides a barrier for electron and hole wavefunction separation in the emitting phase, effectively increasing the radiative rate to a level that is comparable with that in strongly bound excitonic systems. The matrix-inclusion system is widely used towards this goal; it comprises a continuous conductive phase within which isolated inclusions with smaller bandgaps are embedded (FIG. 4b). Charge carriers are injected electrically into the matrix phase and diffuse through to the lower-energy inclusion phase where they recombine radiatively. The distance between inclusions should be less than the carrier diffusion length to compete efficiently with carrier capture into traps inside the host material. The fabrication of matrix-inclusion systems in epitaxial inorganic LEDs is complex. However, solution-processing enables homogeneous mixing of the host matrix and inclusions through self-assembly.

The best solution-processed OLEDs rely on heterostructuring to overcome non-idealities in their constituent electronic materials. They have emissive phosphor inclusions — typically based on metal-organic molecular complexes — which ensure mixing of the singlet and triplet states and thus provide high photoluminescence quantum yields (PLQY) for radiative efficiency. These materials are embedded in high-mobility small-molecule or polymer matrices for carrier transport^{76,77}. The matrix is designed to transport electrons and holes, and is composed of a single ambipolar phase, or more typically, of two or more materials with carrier-selective transport⁷⁸ (FIG. 4c). The topic of matrix-inclusion systems in OLEDs has been heavily studied and is reviewed elsewhere^{79–81}.

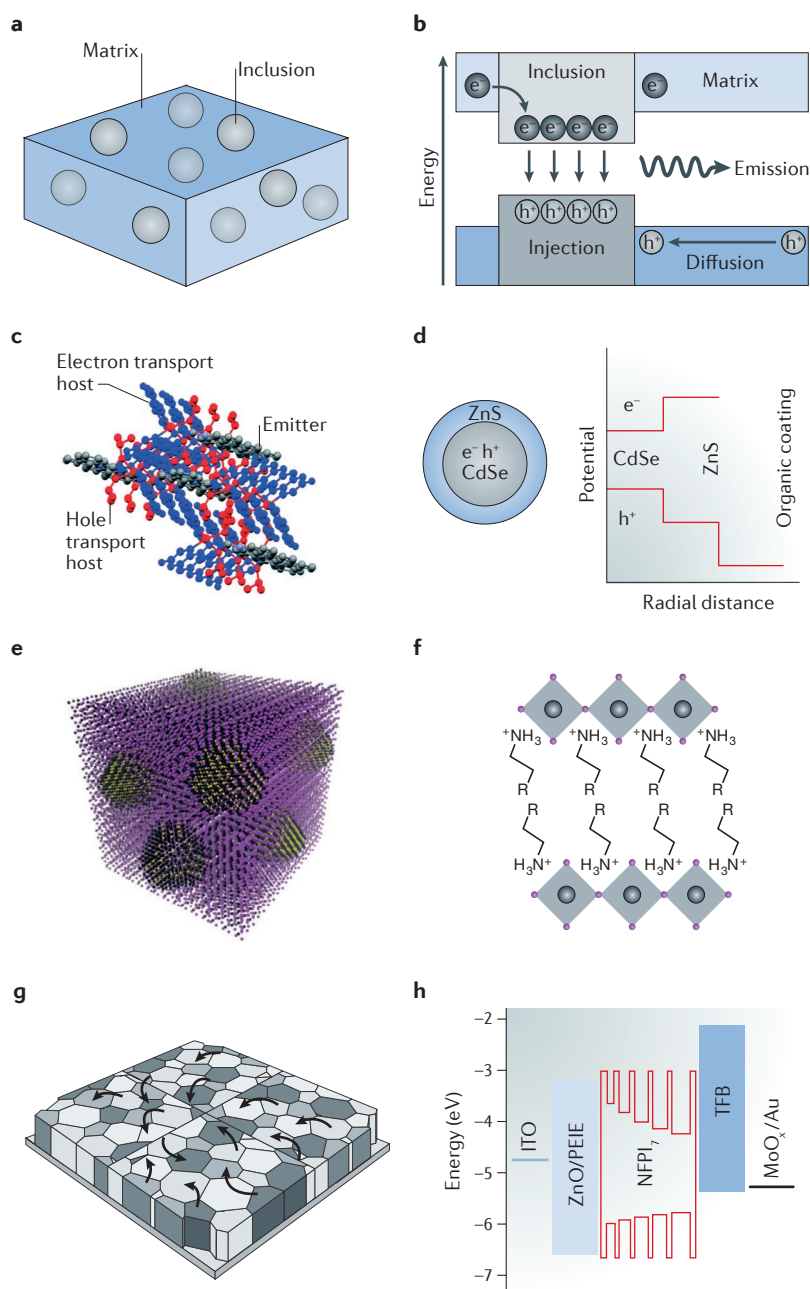


Figure 4 | Heterostructured materials with spatial confinement of carriers for efficient luminescence. **a** | Matrix-inclusion heterostructures. **b** | Type I heterojunction for light-emitting diode (LED) carrier funnelling. **c** | Carrier-selective transport layers for organic LEDs⁷⁸. **d** | Schematic representation of core-shell-ligand colloidal quantum dot (CQD) complexes¹⁰². The energy diagram shows the energy barriers imposed on electrons and holes by the shell and the organic layer. **e** | PbS CQDs embedded in a $\text{CH}_3\text{NH}_3\text{PbI}_3$ matrix⁷³. **f** | 2D-perovskite crystals with layered organic barriers⁹³. **g** | Quasi-2D perovskite heterostructured funnels²⁵. The black arrows indicate the carrier transfer between domains with different bandgaps. **h** | Self-assembled perovskite multi-quantum-well heterostructure LEDs²⁴. ITO, indium tin oxide; NFPI₇, a quasi-2D perovskite; PEIE, poly(ethyleneimine) ethoxylated; TFB, poly(9,9-dioctyl-fluorene-co-N-(4-butylphenyl)diphenylamine). Panel **c** is reproduced with permission from REF. 78, Royal Society of Chemistry. Panel **d** is adapted with permission from REF. 102, InTech. Panel **e** is reproduced from REF. 73, Macmillan Publishers Limited. Panel **f** is reproduced with permission from REF. 93, Royal Society of Chemistry. Panel **g** is reproduced from REF. 25, Macmillan Publishers Limited. Panel **h** is reproduced from REF. 24, Macmillan Publishers Limited.

Leading QD-LEDs are based on heterostructured type I core-shell nanocrystals with organic ligands. Epitaxial wide-bandgap shells can be grown in the solution-phase onto pre-synthesized CQDs with atomic-thickness precision¹³. These composite heterostructured active layers are energetically comparable with a matrix-inclusion system; however, they do not possess a continuous-matrix phase. These materials have three key components. First, the emissive core material is chosen for its luminescence efficiency and colour purity. Second, the choice of shell material is designed for optimal carrier confinement, minimized lattice strain on the core — thereby preserving its optical quality — and conductivity for effective transport. Third, passivating ligands on the surface of the shell are used to reduce the number of trapping states and to control carrier mobility. CdSe nanocrystals with a CdS (REF. 15) or ZnS (REF. 82) shell (FIG. 4d) can achieve peak EQEs of more than 20% at visible wavelengths, and PbS CQDs with a CdS shell have achieved EQEs in excess of 2% in the short-wavelength infrared region⁸³.

Continuous-phase matrix-inclusion systems have shown promise for use in QD-LEDs. Early reports of luminescent CQDs showed that downconversion and electroluminescence can be achieved when the nanocrystals are embedded in an organic matrix^{84–86}. However, this CQD-in-organic-matrix materials platform has yet to gain momentum due to a high density of trap states at the CQD/organic interface. Pure inorganic matrices have also been explored. For example, PbS–CdS core-shell CQDs with an amorphous As_2S_3 matrix were shown to reduce dielectric screening, promoting fast radiative recombination⁸⁷. The growth of a CdS matrix around PbS CQDs by means of the successive ionic layer adsorption and reaction (SILAR) method was shown to increase the solid-state PLQY to 3.7%⁸⁸, compared with less than 1% without encapsulation. However, this luminescence efficiency is still too low to be considered for high-performance QD-LEDs. The purely solution-phase epitaxial growth of shells has benefited from a substantial body of chemical advances, and this approach can now be used to produce trap-minimized interfaces. Although they are promising, post-infiltration strategies such as SILAR have yet to show compellingly high PLQY (and consequently, the electroluminescent quantum yield (ELQY)). This is again ascribed to un-optimized interfaces at the matrix-inclusion boundary.

The matrix-inclusion systems mentioned above suffer from problems in their practical implementation. First, CQDs tend to aggregate during film formation with matrix phases. Second, the interface between the matrix and the CQD surface can be a source of defect states that decreases radiative efficiency. Third, there are only a few solution-processed materials with suitably high mobilities. For example, graphene oxide quantum dots embedded in a poly(*N*-vinylcarbazole) matrix exhibit broadband emission as a result of quantum dot polydispersity and uncontrolled trap-state emission⁸⁹.

Recently, a new hybridized matrix-inclusion platform has emerged: CQDs embedded in a perovskite solid^{73,90} (FIG. 4e). The perovskite and CQDs form a type I

heterojunction for efficient carrier funnelling into CQD emitters, benefiting from efficient electron and hole transport in the perovskite, and resulting in enhanced PLQY compared with CQDs on their own. Furthermore, perovskites used as surface modifiers for quantum dots have been shown to form a heteroepitaxial interface at which CQDs self-align to the perovskite crystal structure, in contrast with strategies that involve amorphous matrices. This material has been used in short-wavelength infrared light-emitting diodes and showed a two-fold improvement over the previous CQD LED power conversion efficiencies in this spectral range⁹¹. Although promising, the materials compatibility between CQDs and perovskites has stringent design requirements. For maximized PLQY, the matrix must be lattice-matched to the CQD surface, thereby minimizing strain. Achieving both lattice matching and sufficient band offsets for carrier confinement is challenging and requires carefully chosen materials and surface engineering.

Perovskites, owing to their excellent transport properties but low exciton binding energy, require heterostructuring to spatially confine carriers for efficient luminescence. One such strategy uses organic ligands to separate the perovskite into 2D platelets (FIG. 4f). By increasing the ratio of ligands to perovskite, the degree of platelet confinement can be tuned, thereby increasing the exciton binding energy at the cost of reduced mobility^{25,92,93}. These heterostructures have been used to form the active layer in efficient and bright perovskite LEDs. Phenylethylammonium iodide ligands have been used to separate $\text{CH}_3\text{NH}_3\text{PbI}_3$ perovskites into 2D perovskite platelets of different thickness and thus different degrees of quantum confinement, creating carrier funnels²⁵ (FIG. 4g). These PeLEDs exhibit a peak EQE and radiance of 8.8% and $80\text{ W sr}^{-1}\text{ m}^{-2}$, respectively. The incorporation of *n*-butylammonium halide precursors into a 3D perovskite solution has been shown to effectively confine carriers to nanometre-sized grains²⁶. These bulk perovskite grains are capped with *n*-butylammonium ligands, facilitating carrier capture and recombination. This led to LEDs with peak EQEs of as high as 10.4%. To date, the most efficient PeLEDs are based on similar multi-quantum-well heterostructures²⁴ (FIG. 4h). In this case, 1-naphthylmethylamine iodide ligands were used to separate formamidinium lead iodide perovskites into self-organized platelets for effective carrier confinement; these PeLEDs exhibited a peak EQE of 11.7% and were demonstrated to be tunable within emission wavelengths of 500–800 nm. Although these reduced-dimensionality perovskite heterostructures are an effective way to increase radiative efficiency, they are still significantly less efficient than OLEDs and QD-LEDs. Harnessing a single continuous transport phase around the light-emitting perovskite domains would be an effective way to improve device performance further.

Conclusions and outlook

Heterostructuring has allowed researchers to control the exciton binding energy and electronic transport properties in solution-processed semiconductors, leading to improved optoelectronic devices. Enhanced solar cells and photodetectors have been realized by combining materials

in the high-binding-energy regime with carrier-selective transport phases. High-efficiency LEDs have been demonstrated by confining active materials with electronic barriers to increase the spatial overlap of electron and hole wavefunctions. To further advance the efficiency of these devices, the organic, CQD and perovskite communities can learn and adapt successful strategies from each other. Combining these distinctly different materials not only expands the configurational space — through the use of binary or even ternary mixtures — but may also help to overcome the practical processing incompatibility limitations for multi-material mixes.

The capacity of mixed-phase materials to provide a more efficient extraction of photogenerated charges has the potential to be further exploited, even in perovskites: BHJs can improve charge extraction from the thick films (in excess of $1\ \mu\text{m}$) that are required for deep infrared or X-ray detection⁹⁴. The use of multiple-ligand mixtures to bind to the same CQD could further advance the efficiency of charge transfer between CQDs by allowing electrons and holes to be bridged by separate ligands, providing a smaller barrier for each carrier.

The capacity to mix two nanomaterials homogeneously without detriment to charge transport alleviates the need for difficult-to-control interpenetrating macroscopic phases that need to be continuous and directly connected to electrodes. For example, mixed CQD–PCBM heterojunctions can be envisioned. Carefully designed CQD–ligand networks with a type II band alignment between the CQD and organic levels could allow for the separation of charge carriers with efficient electron and hole transport through the organic and CQD states, respectively⁹⁵. Taking this concept further, CQDs, nanorods and nanodumbbells enable the fabrication of a heterojunction on a single-entity level⁹⁶, separating the charges and reducing recombination while providing charge transport that is less susceptible to disorder if the insulating ligands are replaced with shorter conductive ones. Another useful property of CQD ligands can be utilized: ligands affect the offset energy of the CQD bands⁹⁷, which allows a BHJ to be developed in a mixture of CQDs of the same type that differ only in their ligands.

Heterostructured materials can further improve photodetection. By utilizing highly absorbing nanostructures combined with a conductive phase, one can realize photodetectors with high internal gain, provided that the band levels are optimized for carrier transfer; the use of colloidal nanoplatelets and quantum dots inside a perovskite matrix provide such natural avenues. The spectral sensitivity can be further expanded to sub-bandgap energies by using intraband transitions, where light excites a carrier from a quantum well into a matrix with an arbitrarily small band offset.

QD-LEDs have reached respectable levels of performance, but stand to learn from concepts used in state-of-the-art OLEDs, which achieve higher EQEs, and PeLEDs, which have demonstrated higher brightness. There has been limited effort towards the fabrication of QD-LEDs with continuous-phase transporting matrices, as are used in OLEDs. Emerging efforts, such as quantum-dot-in-perovskite solids, have shown initial promise

but leave much unexplored. For example, visible-wavelength QD-LEDs are mostly based on zincblende materials and require new compatible constituents for the transport matrix. These materials must have type I band alignment and be as close to lattice-matched as possible. Conductive polymers that are directly coupled to CQD as ligands, or CQD mixtures of different size, material and/or bandgap⁸⁸ coupled using short inorganic ligands⁷⁵ or even fusing^{88,98,99} to ensure conductivity, offer viable pathways to CQD-in-matrix architectures.

PeLEDs are engineered to increase the exciton binding energy of the emitting layer through heterostructuring; however, as has been done for OLEDs, we should strive to achieve continuous transport phases. Charge transport in low-dimensionality perovskite heterostructures has been demonstrated to rely on carrier funnelling^{24,25} in a strongly inhomogeneous energy landscape that arises from a mixture of 2D layers with different degrees of quantum confinement. Matrix-inclusion heterostructures with a continuous transport phase and perovskite emitting layers represent an alternative approach to confining carriers without impeding the transport. A key materials science challenge must be overcome to realize this: the development of controlled phase-separation of perovskites into wide-bandgap matrices. These matrices ideally would comprise wide-bandgap perovskites, but established bipolar organic polymers are also promising (of which

there has been one preliminary study¹⁰⁰). Tuning the halide composition in perovskites is an effective way to control the bandgap; however, influencing phase segregation among these varying-bandgap perovskites has proved to be challenging. Realizing the successful control of phase separation requires new and inventive strategies for precursor development beyond the organic cation crosslinkers used in 2D and quasi-2D perovskites.

Researchers in the field of OLEDs can learn from advances made in QD-LEDs and PeLEDs by working on new materials science to implement higher mobility ambipolar transport materials, such as perovskites. The use of a perovskite transport phase that contains organic inclusions has been explored — an approach that led to an improved luminous output from 2D layered perovskites crosslinked using organic luminophores¹⁰¹. This is a promising approach to improve the brightness of solution-processed OLEDs; however, the materials science for these heterostructures is still undeveloped.

Through materials heterostructuring, solution-processed materials can be used to control the interplay between carrier mobility and exciton binding energy. This enables the design of new materials and optoelectronic devices with enhanced performance. There remain many new materials combinations to explore, and the range of optoelectronic devices that stand to benefit is wide, including photodetectors, solar cells and LEDs.

- Forrest, S. R. The path to ubiquitous and low-cost organic electronic appliances on plastic. *Nature* **428**, 911–918 (2004).
- Shirakawa, H., Louis, E. J., MacDiarmid, A. G., Chiang, C. K. & Heeger, A. J. Synthesis of electrically conducting organic polymers: halogen derivatives of polyacetylene, (CH)_x. *J. Chem. Soc. Chem. Commun.* **1977**, 578–580 (1977).
The discovery of electrically conducting polymers that started the organic electronics era.
- Burroughes, J. H. *et al.* Light-emitting diodes based on conjugated polymers. *Nature* **347**, 539–541 (1990).
One of the first demonstrations of organic LEDs.
- Tessler, N., Denton, G. J. & Friend, R. H. Lasing from conjugated-polymer microcavities. *Nature* **382**, 695–697 (1996).
- Yu, G., Gao, J., Hummelen, J. C., Wudl, F. & Heeger, A. J. Polymer photovoltaic cells: enhanced efficiencies via a network of internal donor–acceptor heterojunctions. *Science* **270**, 1789–1791 (1995).
One of the earliest demonstrations of the BHJ concept that resulted in a breakthrough in polymer solar cell efficiency.
- Aizawa, N. *et al.* Solution-processed multilayer small-molecule light-emitting devices with high-efficiency white-light emission. *Nat. Commun.* **5**, 5756 (2014).
- Li, M. *et al.* Solution-processed organic tandem solar cells with power conversion efficiencies > 12%. *Nat. Photonics* **11**, 85–90 (2016).
- Alexander Efros, L. Interband absorption of light in a semiconductor sphere. *Sov. Phys. Semicond.* **16**, 772–775 (1982).
- Brus, L. E. Electron–electron and electron–hole interactions in small semiconductor crystallites: the size dependence of the lowest excited electronic state. *J. Chem. Phys.* **80**, 4403–4409 (1984).
- Murray, C. B., Norris, D. J. & Bawendi, M. G. Synthesis and characterization of nearly monodisperse CdE (E = sulfur, selenium, tellurium) semiconductor nanocrystallites. *J. Am. Chem. Soc.* **115**, 8706–8715 (1993).
- Hines, M. A. & Scholes, G. D. Colloidal PbS nanocrystals with size-tunable near-infrared emission: observation of post-synthesis self-narrowing of the particle size distribution. *Adv. Mater.* **15**, 1844–1849 (2003).
- Micic, O. I., Curtis, C. J., Jones, K. M., Sprague, J. R. & Nozik, A. J. Synthesis and characterization of InP quantum dots. *J. Phys. Chem.* **98**, 4966–4969 (1994).
- Dabbousi, B. O. *et al.* (CdSe)ZnS core–shell quantum dots: synthesis and characterization of a size series of highly luminescent nanocrystallites. *J. Phys. Chem. B* **101**, 9463–9475 (1997).
- Nozik, A. Quantum dot solar cells. *Phys. E (Amsterdam, Neth.)* **14**, 115–120 (2002).
- Dai, X. *et al.* Solution-processed, high-performance light-emitting diodes based on quantum dots. *Nature* **515**, 96–99 (2014).
- Grim, J. Q. *et al.* Continuous-wave biexciton lasing at room temperature using solution-processed quantum wells. *Nat. Nanotechnol.* **9**, 891–895 (2014).
- Liu, M. *et al.* Hybrid organic–inorganic inks flatten the energy landscape in colloidal quantum dot solids. *Nat. Mater.* **16**, 258–263 (2016).
- Diedenhofen, S. L., Kufer, D., Lasanta, T. & Konstantatos, G. Integrated colloidal quantum dot photodetectors with color-tunable plasmonic nanofocusing lenses. *Light Sci. Appl.* **4**, e234 (2015).
- Kagan, C. R., Mitzi, D. B. & Dimitrakopoulos, C. D. Organic–inorganic hybrid materials as semiconducting channels in thin-film field-effect transistors. *Science* **286**, 945–947 (1999).
This work opened the door to new solution-processed materials (perovskites) that a decade later started a revolution in solution-processed photovoltaics and lighting.
- Era, M., Morimoto, S., Tsutsui, T. & Saito, S. Organic–inorganic heterostructure electroluminescent device using a layered perovskite semiconductor (C₆H₂C₄H₄NH₂)₂PbI₄. *Appl. Phys. Lett.* **65**, 676–678 (1994).
- Lee, M. M., Teuschler, J., Miyasaka, T., Murakami, T. N. & Snaith, H. J. Efficient hybrid solar cells based on meso-superstructured organometal halide perovskites. *Science* **338**, 643–647 (2012).
- Yang, W. S. *et al.* High-performance photovoltaic perovskite layers fabricated through intramolecular exchange. *Science* **348**, 1234–1237 (2015).
- Saliba, M. *et al.* Cesium-containing triple cation perovskite solar cells: improved stability, reproducibility and high efficiency. *Energy Environ. Sci.* **9**, 1989–1997 (2016).
- Wang, N. *et al.* Perovskite light-emitting diodes based on solution-processed self-organized multiple quantum wells. *Nat. Photonics* **10**, 699–704 (2016).
- Yuan, M. *et al.* Perovskite energy funnels for efficient light-emitting diodes. *Nat. Nanotechnol.* **11**, 872–877 (2016).
- Xiao, Z. *et al.* Efficient perovskite light-emitting diodes featuring nanometre-sized crystallites. *Nat. Photonics* **11**, 108–115 (2017).
- Shockley, W. & Read, W. T. Statistics of the recombinations of holes and electrons. *Phys. Rev.* **87**, 835–842 (1952).
- Yuan, Y. *et al.* Ultra-high mobility transparent organic thin film transistors grown by an off-centre spin-coating method. *Nat. Commun.* **5**, 3005 (2014).
- Evers, W. H. *et al.* High charge mobility in two-dimensional percolative networks of PbSe quantum dots connected by atomic bonds. *Nat. Commun.* **6**, 8195 (2015).
- Whitham, K. *et al.* Charge transport and localization in atomically coherent quantum dot solids. *Nat. Mater.* **15**, 557–563 (2016).
- Dou, L. *et al.* 25th anniversary article: a decade of organic/polymeric photovoltaic research. *Adv. Mater.* **25**, 6642–6671 (2013).
A comprehensive review of the current state-of-the-art organic photovoltaics.
- Peet, J. *et al.* Efficiency enhancement in low-bandgap polymer solar cells by processing with alkane dithiols. *Nat. Mater.* **6**, 497–500 (2007).
- Salim, T. *et al.* Solvent additives and their effects on blend morphologies of bulk heterojunctions. *J. Mater. Chem.* **21**, 242–250 (2010).
- Liu, X., Huettnner, S., Rong, Z., Sommer, M. & Friend, R. H. Solvent additive control of morphology and crystallization in semiconducting polymer blends. *Adv. Mater.* **24**, 669–674 (2012).
- Gelinas, S. *et al.* Ultrafast long-range charge separation in organic semiconductor photovoltaic diodes. *Science* **343**, 512–516 (2014).
- Guo, X. *et al.* Polymer solar cells with enhanced fill factors. *Nat. Photonics* **7**, 825–833 (2013).
- Sun, Y. *et al.* Solution-processed small-molecule solar cells with 6.7% efficiency. *Nat. Mater.* **11**, 44–48 (2011).
- Park, S. H. *et al.* Bulk heterojunction solar cells with internal quantum efficiency approaching 100%. *Nat. Photonics* **3**, 297–302 (2009).
- Yang, Y. *et al.* High-performance multiple-donor bulk heterojunction solar cells. *Nat. Photonics* **9**, 190–198 (2015).
- Rath, A. K. *et al.* Solution-processed inorganic bulk nano-heterojunctions and their application to solar cells. *Nat. Photonics* **6**, 529–534 (2012).

41. Rath, A. K. *et al.* Remote trap passivation in colloidal quantum dot bulk nano-heterojunctions and its effect in solution-processed solar cells. *Adv. Mater.* **26**, 4741–4747 (2014).
42. Tan, F. *et al.* Interpenetrated inorganic hybrids for efficiency enhancement of PbS quantum dot solar cells. *Adv. Energy Mater.* **4**, 1400512 (2014).
43. Liu, Z. *et al.* High-efficiency hybrid solar cells based on polymer/PbS_xSe_{1-x} nanocrystals benefiting from vertical phase segregation. *Adv. Mater.* **25**, 5772–5778 (2013).
44. Huynh, W. U., Dittmer, J. J. & Alivisatos, A. P. Hybrid nanorod-polymer solar cells. *Science* **295**, 2425–2427 (2002).
45. Rath, A. K., Bernechea, M., Martinez, L. & Konstantatos, G. Solution-processed heterojunction solar cells based on p-type PbS quantum dots and n-type Bi₂S₃ nanocrystals. *Adv. Mater.* **23**, 3712–3717 (2011).
46. Saha, S. K., Bera, A. & Pal, A. J. Improvement in PbS-based hybrid bulk-heterojunction solar cells through band alignment via bismuth doping in the nanocrystals. *ACS Appl. Mater. Interfaces* **7**, 8886–8893 (2015).
47. Choi, J. J. *et al.* Photogenerated exciton dissociation in highly coupled lead salt nanocrystal assemblies. *Nano Lett.* **10**, 1805–1811 (2010). **This work explores the role of ligand length on the interplay between exciton binding energy and mobility in quantum dot solids, the possibility of exciton dissociation, and thus the key difference between nanocrystalline and organic photovoltaics.**
48. Zhitomirsky, D. *et al.* Engineering colloidal quantum dot solids within and beyond the mobility-invariant regime. *Nat. Commun.* **5**, 3803 (2014). **This work explores the limiting factors for nanocrystal photovoltaic performance, showing the importance of electronic traps as opposed to carrier mobility.**
49. Ip, A. H. *et al.* Infrared colloidal quantum dot photovoltaics via coupling enhancement and agglomeration suppression. *ACS Nano* **9**, 8833–8842 (2015).
50. Carey, G. H., Levina, L., Comin, R., Voznyy, O. & Sargent, E. H. Record charge carrier diffusion length in colloidal quantum dot solids via mutual dot-to-dot surface passivation. *Adv. Mater.* **27**, 3325–3330 (2015).
51. Yang, Z. *et al.* Colloidal quantum dot photovoltaics enhanced by perovskite shelling. *Nano Lett.* **15**, 7539–7543 (2015).
52. Neo, D. C. J. *et al.* Influence of shell thickness and surface passivation on PbS/CdS core/shell colloidal quantum dot solar cells. *Chem. Mater.* **26**, 4004–4013 (2014).
53. Scheele, M., Brütting, W. & Schreiber, F. Coupled organic–inorganic nanostructures (COIN). *Phys. Chem. Chem. Phys.* **17**, 97–111 (2014).
54. Scheele, M. *et al.* PbS nanoparticles capped with tetrathiafulvalenetetracarboxylate: utilizing energy level alignment for efficient carrier transport. *ACS Nano* **8**, 2532–2540 (2014).
55. André, A. *et al.* Toward conductive mesocrystalline assemblies: PbS nanocrystals cross-linked with tetrathiafulvalene dicarboxylate. *Chem. Mater.* **27**, 8105–8115 (2015).
56. Kovalenko, M. V., Scheele, M. & Talapin, D. V. Colloidal nanocrystals with molecular metal chalcogenide surface ligands. *Science* **324**, 1417–1420 (2009). **The first demonstration of a solution-phase ligand exchange to small molecular and atomic ligands, expanding the library of solvents for quantum dots and allowing for much enhanced electrical conductivity of quantum dot solids.**
57. Ning, Z., Dong, H., Zhang, Q., Voznyy, O. & Sargent, E. H. Solar cells based on inks of n-type colloidal quantum dots. *ACS Nano* **8**, 10321–10327 (2014).
58. Fischer, A. *et al.* Directly deposited quantum dot solids using a colloidally stable nanoparticle ink. *Adv. Mater.* **25**, 5742–5749 (2013).
59. Zhang, H., Jang, J., Liu, W. & Talapin, D. V. Colloidal nanocrystals with inorganic halide, pseudohalide, and halometallate ligands. *ACS Nano* **8**, 7359–7369 (2014).
60. Kramer, I. J. *et al.* Ordered nanopillar structured electrodes for depleted bulk heterojunction colloidal quantum dot solar cells. *Adv. Mater.* **24**, 2315–2319 (2012).
61. Lan, X. *et al.* Self-assembled, nanowire network electrodes for depleted bulk heterojunction solar cells. *Adv. Mater.* **25**, 1769–1773 (2013).
62. Jean, J. *et al.* ZnO nanowire arrays for enhanced photocurrent in PbS quantum dot solar cells. *Adv. Mater.* **25**, 2790–2796 (2013).
63. Kim, H.-S. *et al.* Lead iodide perovskite sensitized all-solid-state submicron thin film mesoscopic solar cell with efficiency exceeding 9%. *Sci. Rep.* **2**, 591 (2012).
64. Burschka, J. *et al.* Sequential deposition as a route to high-performance perovskite-sensitized solar cells. *Nature* **499**, 316–319 (2013).
65. Li, X. *et al.* Improved performance and stability of perovskite solar cells by crystal crosslinking with alkylphosphonic acid ω-ammonium chlorides. *Nat. Chem.* **7**, 703–711 (2015).
66. Stranks, S. D. *et al.* Electron–hole diffusion lengths exceeding 1 micrometer in an organometal trihalide perovskite absorber. *Science* **342**, 341–344 (2013).
67. Shi, D. *et al.* Low trap-state density and long carrier diffusion in organolead trihalide perovskite single crystals. *Science* **347**, 519–522 (2015). **The first solution-processed single-crystal lead halide perovskites with electronic properties approaching those of ultrahigh purity conventional bulk semiconductors.**
68. Xing, G. *et al.* Long-range balanced electron- and hole-transport lengths in organic–inorganic CH₃NH₃PbI₃. *Science* **342**, 344–347 (2013).
69. Wang, Z. *et al.* Efficient and air-stable mixed-cation lead mixed-halide perovskite solar cells with n-doped organic electron extraction layers. *Adv. Mater.* **29**, 1604186 (2016).
70. Konstantatos, G. *et al.* Hybrid graphene–quantum dot phototransistors with ultrahigh gain. *Nat. Nanotechnol.* **7**, 363–368 (2012).
71. Saran, R., Stolojan, V. & Curry, R. J. Ultrahigh performance C₆₀ nanorod large area flexible photoconductor devices via ultralow organic and inorganic photodoping. *Sci. Rep.* **4**, 5041 (2014).
72. Garcia de Arquer, F. P. *et al.* Field-emission from quantum-dot-in-perovskite solids. *Nat. Commun.* **8**, 14757 (2016).
73. Ning, Z. *et al.* Quantum-dot-in-perovskite solids. *Nature* **525**, 324–328 (2015). **One of the first demonstrations of a truly hybrid material in which two disparate materials, lead sulfide and perovskite, are intimately matched to form light-emissive quantum dots inside a conductive matrix.**
74. Lin, Q., Armin, A., Burn, P. L. & Meredith, P. Filterless narrowband visible photodetectors. *Nat. Photonics* **9**, 687–694 (2015).
75. Lee, J.-S., Kovalenko, M. V., Huang, J., Chung, D. S. & Talapin, D. V. Band-like transport, high electron mobility and high photoconductivity in all-inorganic nanocrystal arrays. *Nat. Nanotechnol.* **6**, 348–352 (2011).
76. Lee, C. W. & Lee, J. Y. High quantum efficiency in solution and vacuum processed blue phosphorescent organic light emitting diodes using a novel benzofuropridine-based bipolar host material. *Adv. Mater.* **25**, 596–600 (2013).
77. Perumal, A. *et al.* High-efficiency, solution-processed, multilayer phosphorescent organic light-emitting diodes with a copper thiocyanate hole-injection/hole-transport layer. *Adv. Mater.* **27**, 93–100 (2015).
78. Feng, Y. *et al.* A novel bipolar phosphorescent host for highly efficient deep-red OLEDs at a wide luminance range of 1000–10,000 cd m⁻². *Chem. Commun.* **51**, 12544–12547 (2015).
79. Yook, K. S. & Lee, J. Y. Small molecule host materials for solution processed phosphorescent organic light-emitting diodes. *Adv. Mater.* **26**, 4218–4233 (2014).
80. Li, W., Li, J. & Wang, M. Organic host materials for solution-processed phosphorescent organic light-emitting diodes. *Isr. J. Chem.* **54**, 867–884 (2014).
81. Ho, S., Liu, S., Chen, Y. & So, F. Review of recent progress in multilayer solution-processed organic light-emitting diodes. *J. Photonics Energy* **5**, 057611 (2015).
82. Yang, Y. *et al.* High-efficiency light-emitting devices based on quantum dots with tailored nanostructures. *Nat. Photonics* **9**, 259–266 (2015).
83. Supran, G. J. *et al.* High-performance shortwave-infrared light-emitting devices using core–shell (PbS–CdS) colloidal quantum dots. *Adv. Mater.* **27**, 1437–1442 (2015).
84. Tessler, N. Efficient near-infrared polymer nanocrystal light-emitting diodes. *Science* **295**, 1506–1508 (2002).
85. Kang, B.-H. *et al.* Highly efficient hybrid light-emitting device using complex of CdSe/ZnS quantum dots embedded in co-polymer as an active layer. *Opt. Express* **18**, 18303–18311 (2010).
86. Greenham, N. C., Peng, X. & Alivisatos, A. P. Charge separation and transport in conjugated-polymer/semiconductor-nanocrystal composites studied by photoluminescence quenching and photoconductivity. *Phys. Rev. B* **54**, 17628–17637 (1996).
87. Kovalenko, M. V., Schaller, R. D., Jarzab, D., Loi, M. A. & Talapin, D. V. Inorganically functionalized PbS–CdS colloidal nanocrystals: integration into amorphous chalcogenide glass and luminescent properties. *J. Am. Chem. Soc.* **134**, 2457–2460 (2012).
88. Moroz, P. *et al.* Infrared emitting PbS nanocrystal solids through matrix encapsulation. *Chem. Mater.* **26**, 4256–4264 (2014).
89. Kyu Kim, J. *et al.* Origin of white electroluminescence in graphene quantum dots embedded host/guest polymer light emitting diodes. *Sci. Rep.* **5**, 11032 (2015).
90. Ngo, T. T., Suarez, I., Sanchez, R. S., Martinez-Pastor, J. P. & Mora-Sero, I. Single step deposition of an interacting layer of a perovskite matrix with embedded quantum dots. *Nanoscale* **8**, 14379–14383 (2016).
91. Gong, X. *et al.* Highly efficient quantum dot near-infrared light-emitting diodes. *Nat. Photonics* **10**, 253–257 (2016).
92. Quan, L. N. *et al.* Ligand-stabilized reduced-dimensionality perovskites. *J. Am. Chem. Soc.* **138**, 2649–2655 (2016).
93. Sapori, D., Kepenekian, M., Pedesseau, L., Katan, C. & Even, J. Quantum confinement and dielectric profiles of colloidal nanoplatelets of halide inorganic and hybrid organic–inorganic perovskites. *Nanoscale* **8**, 6369–6378 (2016).
94. Yakunin, S. *et al.* Detection of X-ray photons by solution-processed lead halide perovskites. *Nat. Photonics* **9**, 444–449 (2015).
95. Li, H., Wu, Z., Zhou, T., Sellinger, A. & Lusk, M. T. Double superexchange in quantum dot mesomaterials. *Energy Environ. Sci.* **7**, 1023–1028 (2014).
96. Dasgupta, U., Bera, A. & Pal, A. J. *pn*-Junction nanorods in a polymer matrix: a paradigm shift from conventional hybrid bulk-heterojunction solar cells. *Sol. Energy Mater. Sol. Cells* **143**, 319–325 (2015).
97. Brown, P. R. *et al.* Energy level modification in lead sulfide quantum dot thin films through ligand exchange. *ACS Nano* **8**, 5863–5872 (2014).
98. Dolzhenkov, D. S. *et al.* Composition-matched molecular ‘soldiers’ for semiconductors. *Science* **347**, 425–428 (2015).
99. Panthani, M. G. *et al.* High efficiency solution processed sintered CdTe nanocrystal solar cells: the role of interfaces. *Nano Lett.* **14**, 670–675 (2014).
100. Di, D. *et al.* Size-dependent photon emission from organometal halide perovskite nanocrystals embedded in an organic matrix. *J. Phys. Chem. Lett.* **6**, 446–450 (2015).
101. Jemli, K. *et al.* Two-dimensional perovskite activation with an organic luminophore. *ACS Appl. Mater. Interfaces* **7**, 21763–21769 (2015).
102. Jasim, K. E. in *Solar Cells — New Approaches and Reviews* Ch. 11 (ed. Kosyachenko, L. A.) (Intech, 2015).
103. Köhler, A. Organic semiconductors: no more breaks for electrons. *Nat. Mater.* **11**, 836–837 (2012).
104. Kraner, S., Scholz, R., Koerner, C. & Leo, K. Design proposals for organic materials exhibiting a low exciton binding energy. *J. Phys. Chem. C* **119**, 22820–22825 (2015).
105. Yazdani, N., Bozyigit, D., Yarema, O., Yarema, M. & Wood, V. Hole mobility in nanocrystal solids as a function of constituent nanocrystal size. *J. Phys. Chem. Lett.* **5**, 3522–3527 (2014).
106. Meulenbergh, R. W. *et al.* Determination of the exciton binding energy in CdSe quantum dots. *ACS Nano* **3**, 325–330 (2009).
107. Leijtens, T. *et al.* Electronic properties of meso-structured and planar organometal halide perovskite films: charge trapping, photodoping, and carrier mobility. *ACS Nano* **8**, 7147–7155 (2014).
108. Miyata, A. *et al.* Direct measurement of the exciton binding energy and effective masses for charge carriers in organic–inorganic tri-halide perovskites. *Nat. Phys.* **11**, 582–587 (2015).

Competing interests statement

The authors declare no competing interests.

Publisher's note

Springer Nature remains neutral with regard to jurisdictional claims in published maps and institutional affiliations.

How to cite this article

Voznyy, O. *et al.* Engineering charge transport by heterostructuring solution-processed semiconductors. *Nat. Rev. Mater.* **2**, 17026 (2017).